



HAL
open science

Sensitivity of three Mediterranean heavy rain events to two different sea surface fluxes parameterizations in high-resolution numerical modeling

Cindy Lebeaupin Brossier, Véronique Ducrocq, Hervé Giordani

► **To cite this version:**

Cindy Lebeaupin Brossier, Véronique Ducrocq, Hervé Giordani. Sensitivity of three Mediterranean heavy rain events to two different sea surface fluxes parameterizations in high-resolution numerical modeling. *Journal of Geophysical Research: Atmospheres*, 2008, 113, pp.D21109. 10.1029/2007JD009613 . meteo-00337123

HAL Id: meteo-00337123

<https://meteofrance.hal.science/meteo-00337123>

Submitted on 22 Nov 2021

HAL is a multi-disciplinary open access archive for the deposit and dissemination of scientific research documents, whether they are published or not. The documents may come from teaching and research institutions in France or abroad, or from public or private research centers.

L'archive ouverte pluridisciplinaire **HAL**, est destinée au dépôt et à la diffusion de documents scientifiques de niveau recherche, publiés ou non, émanant des établissements d'enseignement et de recherche français ou étrangers, des laboratoires publics ou privés.

Copyright

Sensitivity of three Mediterranean heavy rain events to two different sea surface fluxes parameterizations in high-resolution numerical modeling

C. Lebeaupin Brossier,¹ V. Ducrocq,¹ and H. Giordani¹

Received 16 November 2007; revised 19 March 2008; accepted 26 June 2008; published 6 November 2008.

[1] The southeast of France is prone to heavy rain events during the fall season. For these extreme precipitating events, the Mediterranean Sea supplies heat and moisture to the atmospheric boundary layer through the turbulent heat fluxes. In turn the low-level jet, which frequently accompanies these events, induces a stress on the oceanic mixed layer. The aim of this study is to examine the sensitivity of short-range (24 h) high-resolution (2–3 km) forecasts to the sea surface fluxes parameterization for three representative torrential rainfall events. We consider in particular two sea surface fluxes bulk parameterizations: the original MESO-NH model parameterization based on the Louis (1979) formulation and the iterative Coupled Ocean-Atmosphere Response Experiment (COARE) bulk algorithm from Fairall et al. (2003). Results show that the two parameterizations produce very different air-sea fluxes values, especially for strong winds; the largest differences are therefore found under the low-level jets, where the COARE parameterization reduces the wind stress and the latent heat flux. The evaporation reduction results in a decrease of the low-level humidity transport over the Mediterranean Sea in every case studied so that the convective activity, still intense, results in lower rainfall amounts. The impact of surface fluxes parameterization on the ocean mixed layer modeling is also examined by driving a one-dimensional ocean model with the same set of atmospheric parameters but using the two parameterizations. Results show a significant impact on the mixed layer depth.

Citation: Lebeaupin Brossier, C., V. Ducrocq, and H. Giordani (2008), Sensitivity of three Mediterranean heavy rain events to two different sea surface fluxes parameterizations in high-resolution numerical modeling, *J. Geophys. Res.*, *113*, D21109, doi:10.1029/2007JD009613.

1. Introduction

[2] During the fall season, northwestern Mediterranean regions are prone to heavy rainfall characterized by large totals that may accumulate when one or several frontal systems stay over the area during several days. In some other cases, heavy precipitation leading to large totals in the Mediterranean basin, i.e., more than 200 mm in less than 1 day, is generated by quasi-stationary Mesoscale Convective Systems (MCS) that stay over the region during several hours. Most often, the meteorological environment of these events is characterized by a moderate to intense low-level onshore jet that transports air masses warmed and moistened by the Mediterranean Sea toward the continental regions where they feed the convective systems.

[3] The ocean and the atmosphere exchange energy in the form of heat, humidity and momentum, in proportions that depend on the air-sea interface conditions (oceanic surface

temperature, salinity, current and atmospheric low-level temperature, humidity and wind). The energy exchanges tend to balance the vertical gradients between the Atmospheric Boundary Layer (ABL) and the Oceanic Mixed Layer (OML). The Sea Surface Temperature (SST) is the basic variable, that together with the low-level atmospheric variables (wind, temperature and humidity) couples the atmosphere with the ocean. At midlatitudes, variations in SST and in the mesoscale transfer of heat, moisture and momentum have a key role in the ABL dynamics and thermodynamics, especially during cyclogenesis [*Giordani and Caniaux*, 2001]. The ABL modifications produce in turn feedbacks on the temperature, density and mixing within the OML. The mixing in the oceanic boundary layer is very sensitive to the stress forcing. For example, *Giordani et al.* [2006] have shown that the surface wind stress can be trapped into oceanic mesoscale and submesoscale dynamical structures (as for example mixed-layer depth anomalies, anticyclonic eddy, SST front) that could induce vertical velocities stronger than the well-known *Ekman* [1905] pumping.

[4] On the basis of convective-scale numerical simulations of three torrential rainfall events, *Lebeaupin et al.*

¹Centre National de Recherches, Météorologiques/Groupe d'Etude de l'Atmosphère Météorologique, Météo-France/CNRS, Toulouse, France.

[2006] (hereafter LE06) show that a warmer Mediterranean SST increases sea surface heat fluxes, which in turn moisten and destabilize atmospheric low levels and intensify the convection and the surface rainfall totals. Conversely, the atmospheric convection could disappear after a few hours of simulation with a cooler SST owing to weaker sea surface heat fluxes that reduce the available convective energy. However, the analysis of the sensitivity to SST cannot be completely isolated from how the air-sea fluxes are parameterized within the atmospheric model. Indeed, the energy exchange between the ocean and the atmosphere is very sensitive to the surface fluxes parameterization [Webster and Lukas, 1992]. An accurate parameterization of sea surface turbulent fluxes, that are the latent and sensible heat fluxes as well as the momentum flux (also called wind stress), is fundamental for a correct evaluation of the energy transfers at the air-sea interface.

[5] Sea surface fluxes parameterizations in numerical models are based on bulk algorithms, that differ in the formulation of the transfer coefficients and in the treatment of surface roughness lengths as well as how they take into account wave spectrum, sea spray, salinity of sea water, convective gustiness or capillary waves [Brunke *et al.*, 2002]. A very great attention is paid to the parameterizations validity, in particular by comparison of the calculated fluxes against the measured ones. However, many problems still remain in the measurement of air-sea fluxes, particularly at low or high wind speed or under strong stratification. Data measurement processing needs also to address the dependence and effects of the sea state in the various methods used to measure turbulent parameters as well as the airflow distortions around ships or sensors. These problems could be passed on parameterization validation, and finally in the way to represent fluxes in numerical models or climatologies [Weill *et al.*, 2003].

[6] In this paper, two fundamentally different bulk parameterizations are used to evaluate the sensitivity to the sea surface fluxes formulation of Mediterranean torrential rain events and more specifically of their high-resolution (2–3 km) modeling. Three cases of heavy precipitation events are examined. They are the same as those selected by LE06 for examining the sensitivity to the SST. The model used is the French research high-resolution and nonhydrostatic model MESO-NH in the same configuration as LE06. Besides the original bulk parameterization of the MESO-NH model based on the *Louis* [1979] formulation and used by LE06, we consider also here the iterative bulk algorithm developed by *Fairall et al.* [1996] during the Coupled Ocean-Atmosphere Response Experiment (COARE) of the Tropical Ocean Global Atmosphere (TOGA) research program [Webster and Lukas, 1992]. The COARE algorithm is updated since *Fairall et al.* [2003] and is now one of the most frequently used algorithms in the air-sea interactions' community [Weller *et al.*, 2004]. Moreover the intercomparison study of *Brunke et al.* [2003] between twelve ocean surface turbulent fluxes bulk algorithms, ranked the COARE bulk algorithm as a very efficient algorithm partly caused by its 3.0 revision utilizing data from both the tropics and midlatitudes to extend its validity to higher wind regimes.

[7] This study aims at evaluating the sensitivity to these two different surface fluxes parameterizations for atmospheric and oceanic conditions encountered during Mediterranean heavy precipitation events. Kilometric-scale atmospheric simulations of three exceptional precipitation events are performed using alternatively the two parameterizations. The characteristics of the two bulk air-sea fluxes parameterizations are described in section 2, whereas the experimental design is presented in section 3. Impacts on the atmospheric boundary layer as well as on the simulation of the precipitating systems are then discussed in section 4. Then section 5 describes the influence of the two parameterizations on the ocean mixed layer associated with Mediterranean heavy precipitation events based on one-dimensional (1-D) ocean mixed layer simulations for one of the events. Conclusion and outlooks follow in section 6.

2. Bulk Air-Sea Fluxes Parameterization

[8] The original MESO-NH parameterization and the COARE 3.0 algorithm used in this study are both bulk parameterizations. The bulk aerodynamic algorithms relate the turbulent fluxes to bulk meteorological variables (e.g., surface air temperature, humidity and wind, and sea surface temperature) using the *Monin-Obukhov* [1954] similarity theory (MOST). The turbulent fluxes are directly related to meteorological variables by defining turbulent exchange coefficients that link surface fluxes to mean meteorological vertical gradients between the surface and the measurement level or the lowest model level. Thus, the turbulent surface fluxes, for example, the momentum flux τ (or wind stress), the sensible heat flux H , and the latent heat flux LE , defined positive toward the atmosphere are given by

$$\tau = -\rho_a u_*^2 = -\rho_a C_D S^2 \quad (1)$$

$$H = \rho_a c_p u_* \theta_* = \rho_a C_H S (\theta_a - \theta_s) \quad (2)$$

$$LE = \rho_a c_p u_* q_* = \rho_a C_E S (q_a - q_s), \quad (3)$$

where C_D , C_H and C_E are the exchange coefficients for wind, heat and evaporation respectively; ρ_a is the density of air; S is the relative near-surface wind speed; θ_a and θ_s are the atmospheric and surface potential temperatures, respectively; q_a and q_s are the atmospheric and surface specific humidities, respectively; u_* , θ_* and q_* are the scaling parameters for wind, potential temperature and humidity, respectively.

[9] Bulk algorithms differ in how the above exchange coefficients are parameterized. Other differences include those in considering or not convective gustiness in the wind speed S and salinity of seawater in the calculation of q_s as well as how roughness lengths are parameterized.

[10] For the both parameterizations used in this study, the transfer coefficients are partitioned into individual profile components,

$$C_X = c_x^{1/2} c_d^{1/2}, \quad (4)$$

in which c_x , the bulk transfer coefficient for the variable x ($x = d$ for wind, h for heat and e for evaporation), is itself function of the surface stability following the Monin-Obukov similarity theory (hereafter MOST),

$$c_x^{1/2}(\zeta) = c_{xn}^{1/2} F_x \left(\zeta, \kappa, c_{xn}^{\frac{1}{2}} \right) \quad (5)$$

$$c_{xn}^{1/2} = \frac{\kappa}{\ln \left(\frac{z}{z_{0x}} \right)}, \quad (6)$$

where F_x is a function of the MOST stability parameter ζ , the Von Karman's constant κ , the height z of measurement (or the lowest model level) of the mean quantity and the roughness length z_{0x} for the quantity x . The subscript n refers to neutral stability ($\zeta = 0$). The neutral part of the transfer coefficient c_{xn} depends on the surface roughness lengths which are usually a combination of the Charnock's [1955] expression and the smooth flow limit, following [Smith, 1988]

$$z_0 = \alpha \frac{u_*^2}{g} + b \frac{\nu}{u_*}, \quad (7)$$

with α and b constants and ν the kinematic viscosity of dry air. The main differences between the COARE 3.0 and original MESO-NH algorithms are stressed in the following.

2.1. COARE 3.0 Bulk Algorithm

[11] For the purpose of this study, the COARE 3.0 algorithm has been implemented within the MESO-NH's surface model. This algorithm is one of the most frequently used algorithms in the air-sea interactions' community [Weller *et al.*, 2004]. It has been designed during the Coupled Ocean-Atmosphere Response Experiment (COARE) of the Tropical Ocean Global Atmosphere (TOGA) research program [Webster and Lukas, 1992]. The reader is referred to Fairall *et al.* [1996, 2003] for a comprehensive description of the COARE algorithm and subsequent updated versions. From version 2.5 to 3.0, the performance of the algorithm has been extended by considering cruise data from both the tropics and midlatitudes.

[12] Combining equations (1), (2), (3), and (5) leads to a set of nonlinear equations (see Appendix A) which is solved using an iterative technique in the COARE 3.0 algorithm. Among the possible additional options of the parameterizations, we select a subset that includes the effects of gustiness, precipitation and sea water salinity.

[13] The gustiness velocity is included to take into account the additional flux induced by the boundary layer subgrid-scale variability:

$$S = \sqrt{u^2 + v^2 + w_g^2} \quad (8)$$

$$w_g = \beta w_* = \beta \left(-\frac{g}{\theta_v} \theta_{v*} u_* z_i \right)^{\frac{1}{3}}, \quad (9)$$

with $\beta = 1.2$ and z_i is the depth of the convective boundary layer imposed to 600 m.

[14] Salinity of sea water is also taken into account by multiplying the specific humidity at saturation by the factor 0.98, that corresponds to a reduction of saturated vapor pressure caused by seawater salinity [Kraus, 1972].

[15] The possibility of considering the surface wave influence on roughness lengths has been implemented but not selected here; the velocity roughness length is therefore given here by the well-known Smith's [1988] equation (equation (7)), with $b = 0.11$ and the Charnock's [1955] constant depending on wind speed: α is set to 0.011 for wind speed below 10 m s^{-1} , then increasing linearly up to 0.018 at 18 m s^{-1} , and remaining constant for larger wind speed values. The roughness lengths for heat and moisture are given by

$$z_{0t} = z_{0q} = \min \left(1.1 \times 10^{-5}, 5.5 \times 10^{-5} Re_*^{-0.6} \right)$$

with the Reynolds number Re_* defined as $z_0 u_* / \nu$.

[16] The cooling and stress precipitation fluxes corrections following Gosnell *et al.* [1995] and Fairall *et al.* [1996] are also included.

[17] The main difference between the COARE 3.0 package and the version used in this study is the noninsert of the warm pool and cool skin effects; we assume that the SST simulates by or provided to the ocean and atmospheric models is the "true skin" temperature. As warm layer and cool skin corrections on SST are made in order to take into account the oceanic response to radiative fluxes, and the oceanic model is able to simulate these effects, we do not include the warm layer and cool skin corrections in the COARE parameterization used in our study in order to be consistent for the sea fluxes parameterization used in both the ocean and atmospheric models. Moreover the warm layer and cool skin progressively develop in the tropics under stable meteorological situations, they are less important in midlatitude regions like the Mediterranean basin, especially under unstable conditions as in the convective events studied here.

2.2. Original Parameterization of MESO-NH

[18] The early sea surface flux parameterization implemented within the MESO-NH's surface model is a bulk parameterization based on the Louis [1979] expression. For this parameterization, the previously described iterative algorithm is replaced by an explicit approximation method based on the relationships between the MOST stability parameter and the Richardson Number Ri . The exchange coefficients are therefore expressed as a function of the Richardson number, the roughness lengths and the Von Karman constant. The analytical formulae are detailed in Appendix A. The roughness lengths follow equation (7), but with a zero smooth flow limit term ($b = 0$) and $\alpha = 0.015$. Moreover, contrary to COARE parameterization, the Louis [1979] parameterization does not include any options (no gustiness velocity, no Webb *et al.* [1980] correction and no precipitation effects). A validation of the scheme is provided by Louis [1979], based however only on one-dimensional atmospheric experiments at high latitudes (over the Norwegian Sea). The validation was also limited to evaluate the ability of the sea surface fluxes parameterization to well represent the temperature and humidity diurnal cycle and to

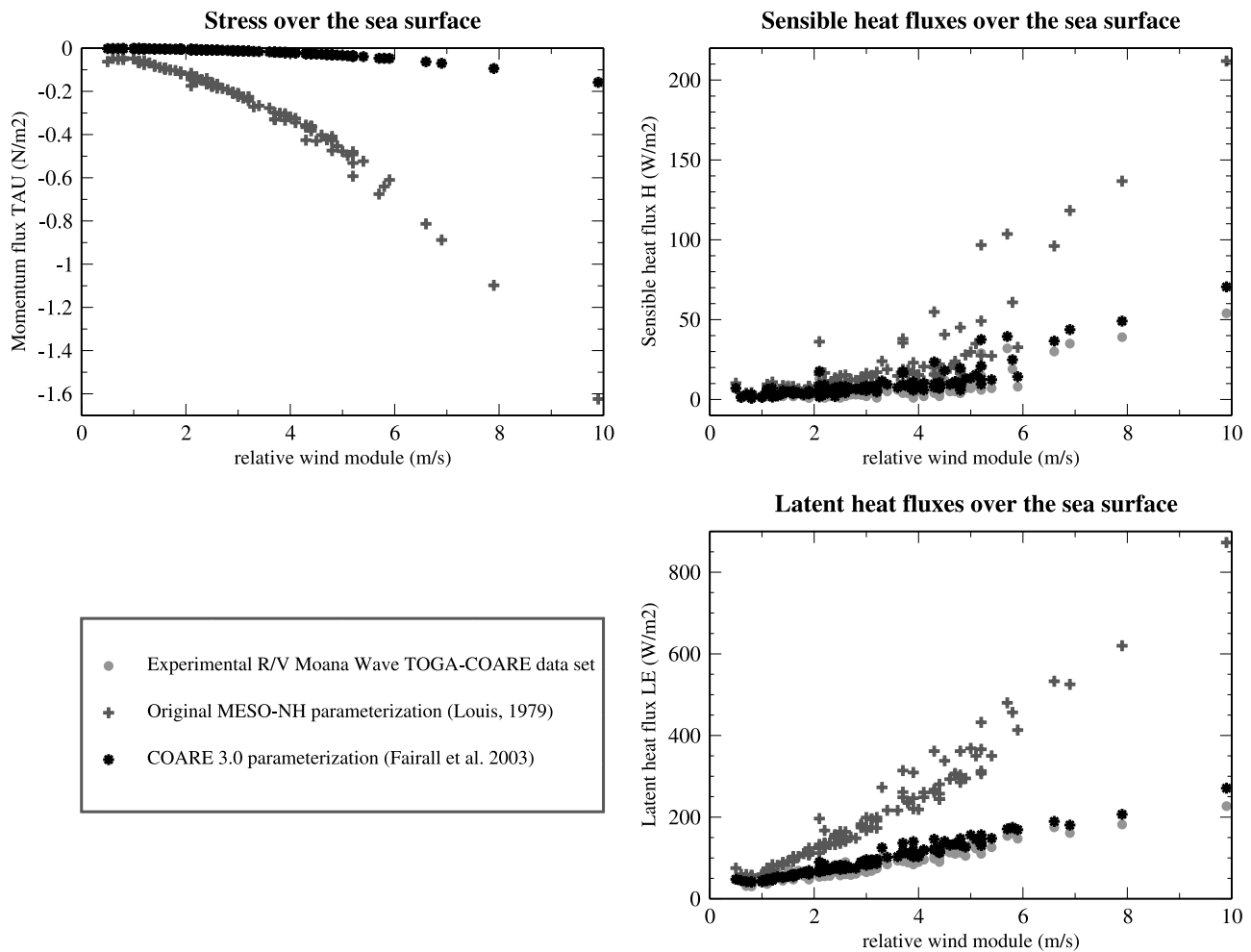


Figure 1. Sea surface fluxes parameterizations comparison using R/V *Moana Wave* data set: latent heat and sensible heat fluxes (in W m^{-2}) and wind stress (in N m^{-2}) in function of wind speed. The experimental fluxes data from TOGA-COARE experiment are plotted as light grey circles, the original MESO-NH parameterization is plotted as grey crosses, and the COARE bulk algorithm is plotted as black stars.

examine its behavior in conditions of strong vertical temperature gradient. Nowadays, more thorough validations of parameterizations are performed, scanning a wide range of stability and wind conditions throughout the world and confronting simulated fluxes to measurements in a consistent way [Weill et al., 2003].

2.3. Comparison on the R/V *Moana Wave* TOGA-COARE Data Set

[19] The two parameterizations have been evaluated on the R/V *Moana Wave* COARE data set [Fairall et al., 1997]. The aim here is to give a first idea of differences between the two parameterizations that could occurred during the numerical simulation integration. The temperature, wind and humidity at measurement height as well as the SST from the R/V *Moana Wave* set have been provided as input to the two parameterizations off-line running. Moreover an experimental turbulent fluxes data set was derived from the Eddy Correlation Method by Fairall et al. [1997]. Consequently, this data set can be considered as an independent reference. Even though this data set is limited

to $0\text{--}10\text{ m s}^{-1}$ wind speed and tropical conditions, significant differences between the two parameterizations can be highlighted. First of all, Figure 1 shows that the COARE 3.0 parameterization fits very well the reference data set even if a slightly modified version neglecting the wave influence and the “cool skin” and “warm layer” effects is implemented in the MESO-NH model. Figure 1 also highlights that the original parameterization of MESO-NH computes unrealistic overestimated values as the wind speed increases, specially for the latent heat flux. This overestimation was already highlighted when comparing the *Louis*’s [1979] parameterized fluxes to observed fluxes data during the CATCH and FASTEX experiments [Eymard et al., 1999] and during the POMME experiment [Caniaux et al., 2005].

3. Experimental Design

3.1. Heavy Precipitation Events

[20] The three heavy precipitation events are the same as LE06. The events, named from the French department (a

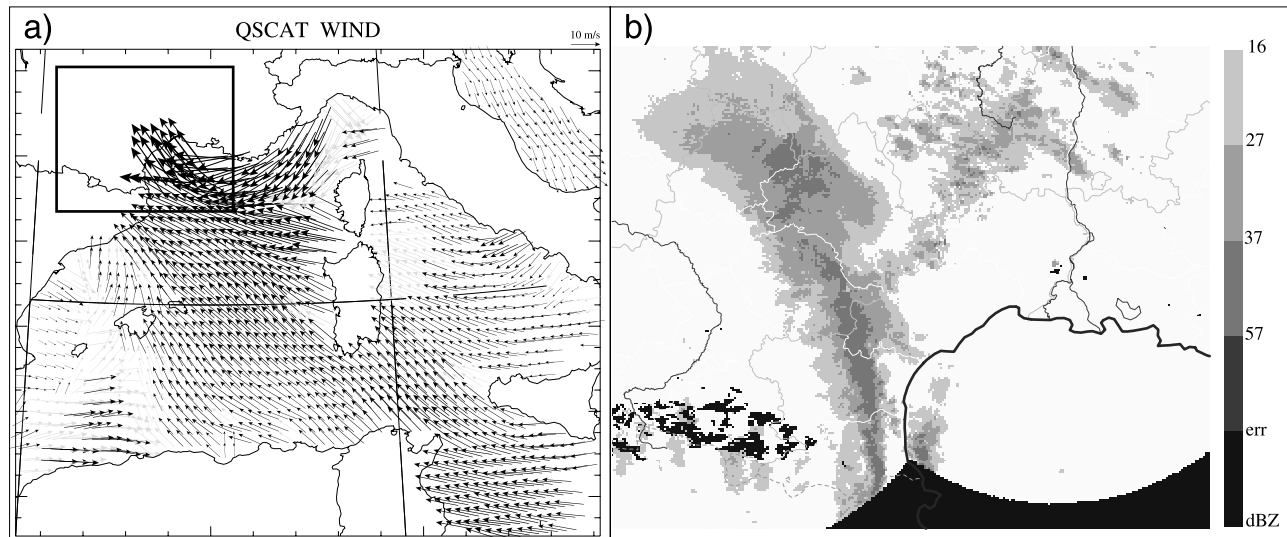


Figure 2. AUDE CASE: (a) 10-m winds from SeaWinds Scatterometer aboard the QuikSCAT at 1806 UT, 12 November 1999; (b) reflectivities (in dBZ) from the ARAMIS radar network at 2330 UT, 12 November 1999. For Figure 2a, the vector scale is given at the top right of the panel; gray vectors are for data with large uncertainties due to clouds over the region.

department is a subdivision of France administered by a prefect) that received the most important precipitation amount, occurred on (1) 12–13 November 1999 (hereafter Aude Case), (2) 8–9 September 2002 (hereafter Gard case), and (3) 3 December 2003 (hereafter Hérault case).

[21] The two first cases are major torrential rain events that occurred over southeastern France; huge precipitation totals (more than 500 mm in less than 24 hours), mainly induced by quasi-stationary mesoscale convective systems, have been recorded. These events resulted in major flash floods with more than 30 and 20 fatalities, respectively. A comprehensive description of these cases is given by *Ducrocq et al.* [2002, 2003] and *Delrieu et al.* [2005]; only a brief overview is given here.

[22] The Aude case was characterized by an upper level low-pressure area centered over Spain on 12 November 1999 at 1200 UT that induced a vast southerly flow from North Africa to southern France. This southerly flow was associated with strong convective available potential energy values as indicated by the upstream Palma sounding at 1200 UT, 12 November 1999 (not shown) [see *Ducrocq et al.*, 2002]. Within the warm air mass transported by the southerly flow, surface lows formed and accelerated the low-level easterly to southeasterly jet over the Mediterranean Sea with winds of more than 25 m s^{-1} (Figure 2a). The convergence is also enhanced by the deflection of the low-level flow by the Southern Alps. The intense convective rainfall started around 1500 UT, 12 November. Convection

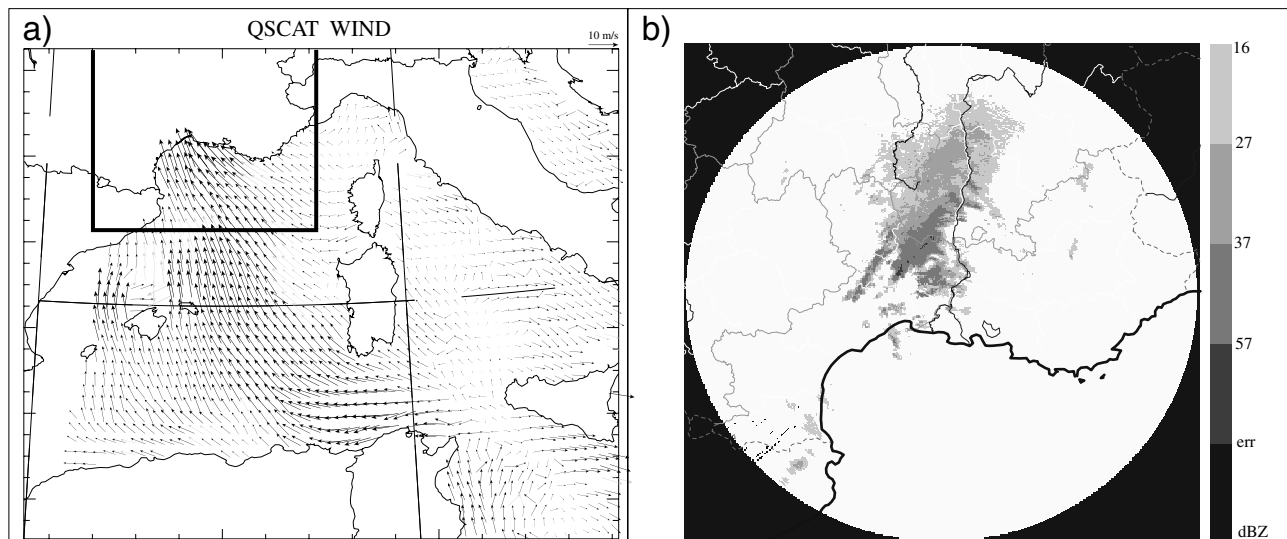


Figure 3. GARD CASE: same as Figure 2, except for (a) 1736 UT, 8 September 2002 and (b) 0155 UT, 9 September 2002.

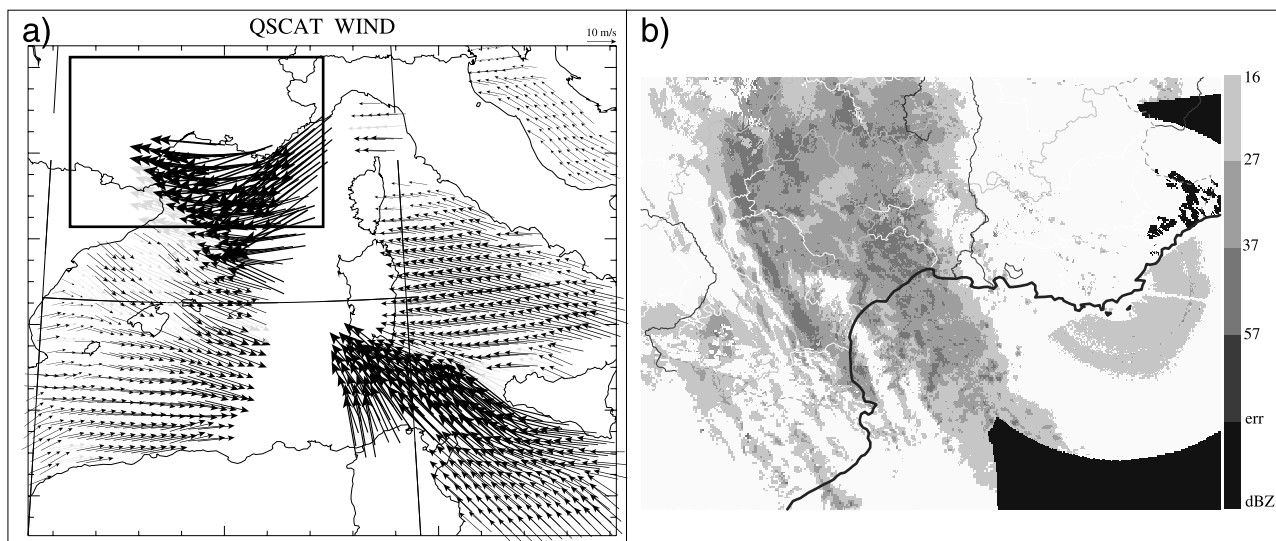


Figure 4. HERAULT CASE: same as Figure 2, except for (a) 1706 UT, 3 December 2003 and (b) 1400 UT, 3 December 2003.

organized in a quasi-stationary mesoscale convective system (MCS) that stayed over the Aude region until 0000 UT (Figure 2b). Most of the high precipitation totals recorded can be attributed to the MCS. The surface rainfall totals reached the maximum value of 624 mm in less than 48 hours in Lézignan-Corbières (Aude department). During the night of 12 to 13 November 1999, the upper level pressure low pivoted, pushing the southerly flow away over north Italy while convection moved eastward, and decayed.

[23] The Gard case was characterized by an upper level cold pressure low centered over Ireland and extending to the Iberian Peninsula during the morning of 8 September 2002, resulting in a southwesterly diffluent flow over southeastern France. Associated with the upper level low-pressure area, a surface cold front undulated over western France. An intense southerly low-level flow, conditionally unstable, established over the French southeastern coast (Figure 3a). First convective cells developed over the Mediterranean Sea around 0400 UT, 8 September 2002, then progressed northward until reaching the continent around 0800 UT. Convection organized in a MCS and became quasi-stationary around 1200 UT. Its convective part affected mainly the Gard region, whereas the stratiform precipitation extended northward (Figure 3b). During the afternoon of 8 September, the cold front progressed slowly to the east while the upper low pivoted to a NW/SE axis. During the night of 8 to 9 September 2002, the cold front and the MCS merged and then moved away from the Gard region in the late morning of 9 September. The precipitating system has stayed over the region for almost 24 hours. During this period, surface rainfall totals reached until 691 mm in 24 hours recorded near the Alès town (Gard Department).

[24] The third case belongs to the other type of meteorological events that lead to flood over the Mediterranean, i.e., frontal systems that stayed over the same region for several days. The Hérault case was characterized by an upper level low-pressure area centered over Spain that established a southerly flow over southern France, and, a slow moving surface frontal system with embedded convection. The cold

surface front stationed over the Gulf of Lions area and southeastern France from 1 to 4 December 2003. The 3 December 2003, which was the most convective day, daily rainfall totals reached about 150 mm. Low-level winds also intensified during this day: easterly wind gusts up to $25\text{--}40\text{ m s}^{-1}$ over the Gulf of Lions were observed (Figure 4a) and a strong swell, with associated beach-combers waves reaching 9 m, disturbed the river water run-off to the sea. The flooding resulted in a major flood of the Rhône river and led to the death of 7 people.

3.2. MESO-NH Model

[25] All atmospheric simulations were performed with the nonhydrostatic mesoscale MESO-NH model [Lafore *et al.*, 1998]. Prognostic variables are the three components of winds, the potential temperature, the turbulent kinetic energy and the mixing ratios of vapor and of five hydrometeors classes (cloud liquid-water, rainwater, primary ice, snow and graupel). The same model configuration as LE06 is used with two interactive nested grids running at horizontal resolution of 9.5 km and 2.4 km respectively, centered over the mesoscale system with location and size depending on the studied case. The subgrid-scale convection is parameterized following Bechtold *et al.* [2001] at 9.5 km resolution whereas no convective scheme is used at 2.4 km. We focus in the following on the 2.4-km domain that covers approximately a $600\text{ km} \times 600\text{ km}$ area around the Gulf of Lions. A bulk microphysical scheme [Pinty and Jabouille, 1998] governs the temporal evolution of the water species.

Table 1. Characteristics of the MESO-NH Simulations

MESO-NH Simulations	Aude Case	Gard Case	Hérault Case
Initial time	12 Nov 1999 1200 UT	8 Sept 2002 1200 UT	3 Dec 2003 0000 UT
Duration, hours	18	24	24
With the original MESO-NH parameterization	ORI	ORI	ORI
With the iterative COARE bulk algorithm v3.0	COA	COA	COA

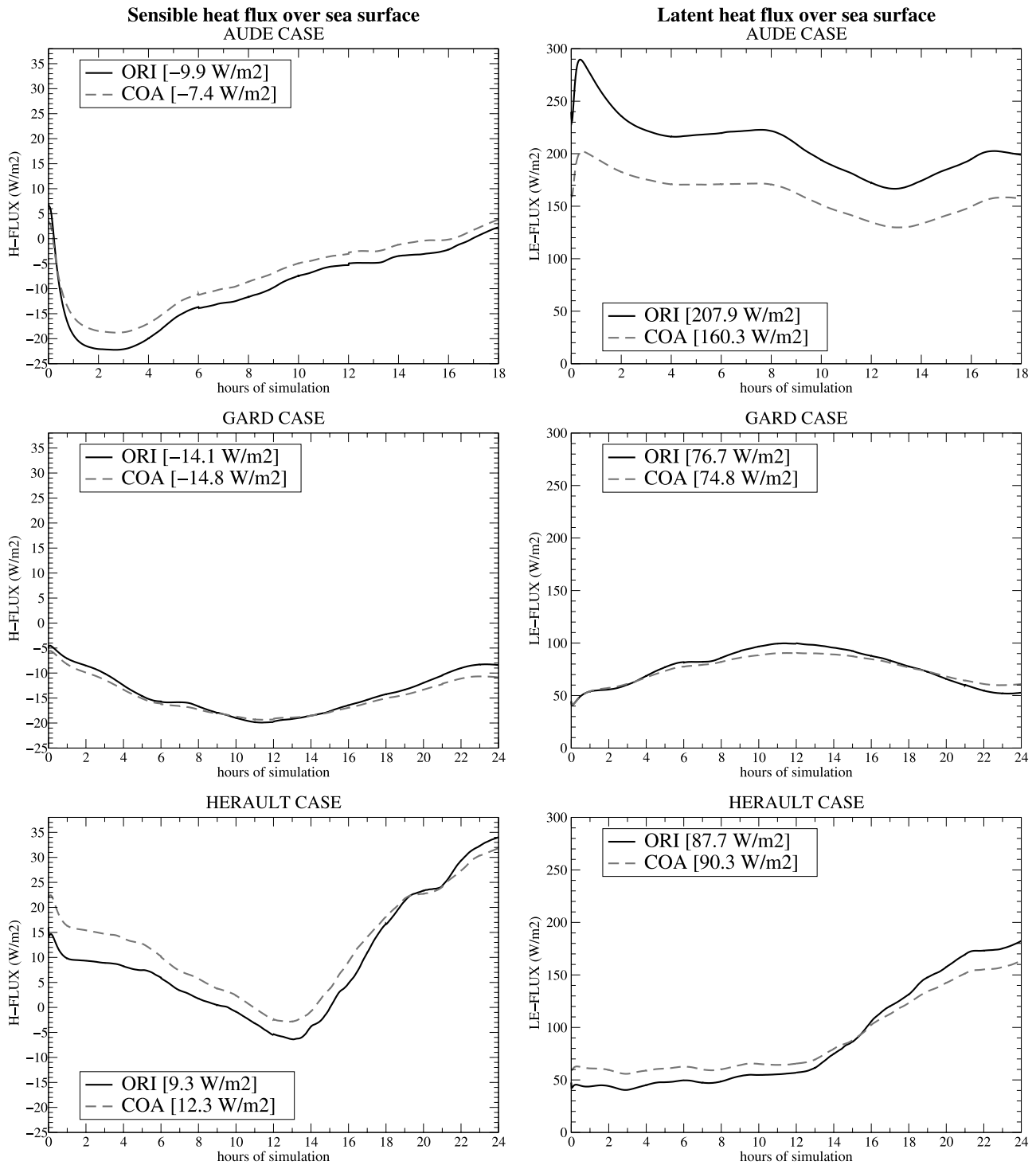


Figure 5. Temporal evolution of sensible (H) and latent (LE) heat fluxes ($W\ m^{-2}$) averaged over the 2.4-km domain sea grid points for the (top) Aude, (middle) Gard and (bottom) Hérault cases. The time average values are indicated in brackets.

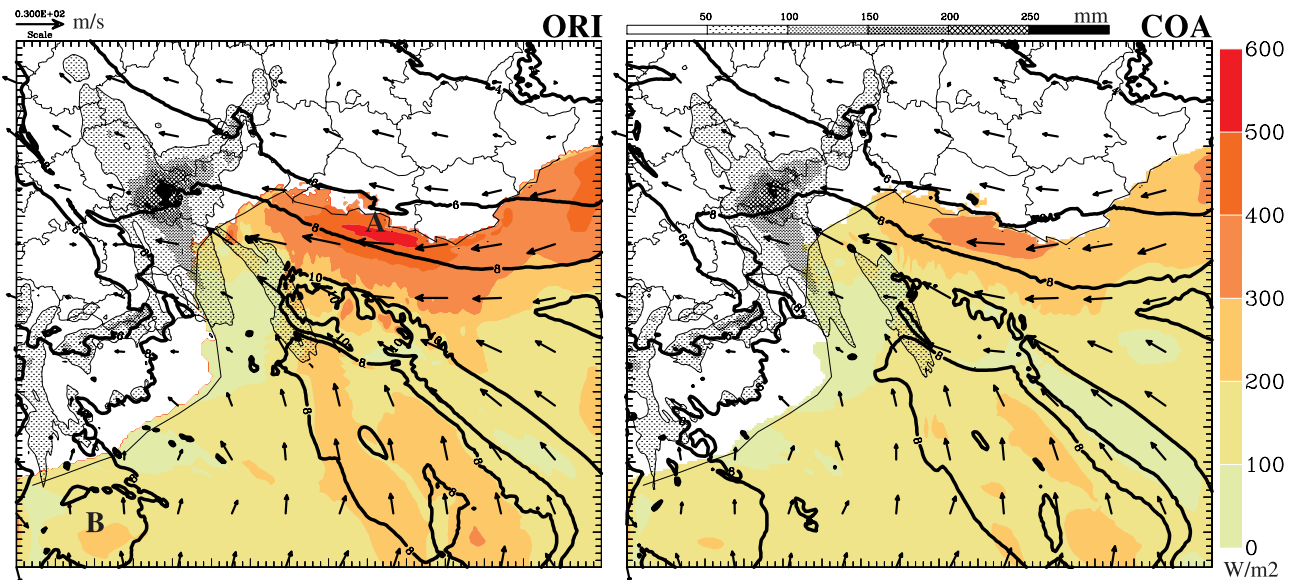


Figure 6. AUDE CASE, 0600 UT, 13 November 1999: latent heat flux (W m^{-2} , right red scale), 30-m AGL horizontal wind vectors (m s^{-1} , top arrow scale), 30-m AGL vapor mixing ratio (g/kg , thick lines), and 18-h accumulated surface rainfall (millimeters, top hatched scale; find maximum values in Table 2) for ORI and COA simulations.

[26] The surface energy exchanges are parameterized according to four different schemes depending on the surface types. The natural land surfaces are handled by the Interactions Soil-Biosphere-Atmosphere (ISBA) scheme [Noilhan and Mahfouf, 1996]. Energy exchanges over town surface are parameterized according to the Town Energy Balance (TEB) scheme [Masson, 2000]. Until today, energy transfers over lakes are computed in the same way as the original MESO-NH surface fluxes parameterization described in section 2.2. For ocean, the both parameterizations have been alternatively used on the three heavy precipitation events (Table 1): ORI experiments use the original MESO-NH sea surface fluxes parameterization [Louis, 1979] and COA the slightly modified version of the iterative COARE bulk algorithm in its last version 3.0 [Fairall et al., 2003] as described in section 2. Initial atmospheric conditions as well as SST are provided by the ARPEGE analyses (Table 1). SST fields do not evolve with time during the very short-range atmospheric simulations (see LE06 for description of the ARPEGE SST).

3.3. One-Dimensional Ocean Model

[27] The impact of the surface fluxes parameterizations on the oceanic mixed layer has been also examined. The one-dimensional kinetic energy model described by Gaspar et al. [1990] has been used for simulations of the oceanic vertical mixing. By analogy with the atmospheric turbulence, this model includes a prognostic equation for the turbulent kinetic energy with a 1.5 closure. The prognostic variables are the temperature, the salinity and the current defined on 40 vertical levels, spaced by 5 m near the air-sea surface up to 1000 m for the deeper ocean.

[28] Latent and sensible heat surface fluxes as well as surface wind stress simulated by both the COARE 3.0 and the original MESO-NH parameterizations from the same

atmospheric simulated parameters have been used to drive the 1-D ocean model during 24 hours on the Hérault case. The ocean temperature and salinity are initialized by a MERCATOR analysis [Bahrel et al., 2004] valid for 0000 UT, 3 December 2003. The current are initially supposed to be null.

4. Impact on Atmospheric Simulations

4.1. Sea Surface Turbulent Fluxes

[29] Figure 5 shows the temporal evolution of sensible (H) and latent (LE) heat fluxes averaged over 2.4-km domain sea grid points for both ORI and COA experiments. The largest difference between the two sets of experiments

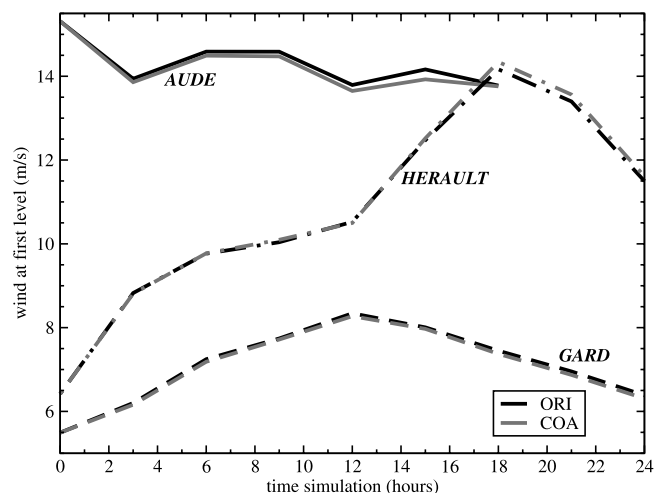


Figure 7. Temporal evolution of the 30-m AGL wind speed averaged over the 2.4-km sea domain.

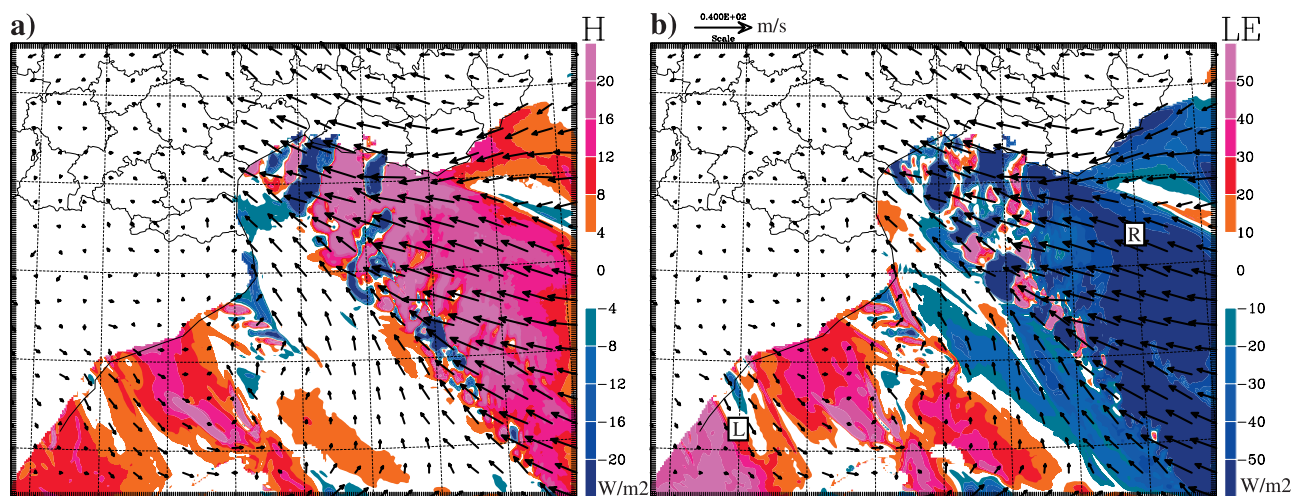


Figure 8. HERAULT CASE, 1500 UT, 3 December 2003: H and LE fluxes differences between COA and ORI experiments (in W m^{-2}) over the 2.4-km sea domain, and 30-m AGL winds (arrows; unit m s^{-1}) simulated by the ORI experiment. Areas where the fluxes simulated by COA are larger than those simulated by ORI are in red tones, whereas where they are weaker, they are in blue tones.

is found for the latent heat fluxes associated with the Aude case: LE is on average weaker by nearly 50 W m^{-2} in COA for that case (Figure 5). The differences are especially large under the low-level jet. Indeed, the Aude case is characterized by strong southeasterly/easterly low-level jets ($\geq 25 \text{ m s}^{-1}$) converging over the Gulf of Lions (Figure 6). Associated with the strong convergent winds, large latent heat fluxes over the sea are therefore simulated, until more than 500 W m^{-2} near the French coasts (labeled A in Figure 6) at 0600 UT, 13 November 1999, in ORI experiment. The COA experiment simulates latent heat fluxes in that area that can be 200 W m^{-2} weaker than the ORI ones. Note that in some area where winds are weak ($< 5 \text{ m s}^{-1}$), LE is slightly larger in COA compared to ORI. For instance, along the Spanish coasts (labeled B in Figure 6), the fluxes are 10 W m^{-2} larger in COA than in ORI. The sensible heat fluxes are not significantly different between the two parameterizations. The differences in average reach only a few W m^{-2} between the two parameterizations for the Aude case (Figure 5), only local differences are present inside the convective system region. Indeed, as the convective cells are not exactly at the same location in the two experiments, their signatures in the latent and sensible heat fluxes fields are also not exactly at the same place in the two experiments, leading to locally significant differences between the two fields (Figure 6).

[30] For the two other cases, differences between COA and ORI latent heat fluxes are weaker (Figure 5), owing to weaker low-level winds over the sea (Figure 7). As the wind is relatively weak over sea during the Gard event, only small local differences for the sensible and latent heat fluxes over sea are therefore found between ORI and COA experiments (Figure 5). For the Hérault case, the winds averaged over the sea increase significantly during the afternoon (Figure 7), resulting in an increase of the latent and sensible heat fluxes (Figure 5). During the morning, as the average winds are rather weak, both latent and heat fluxes simulated by COA are larger than those simulated by ORI. On the opposite during the afternoon, the latent heat fluxes aver-

aged over sea (Figure 5) clearly shows weaker values after 1500 UT in COA, in agreement with the intensification of the southeasterly low-level winds at that time (Figure 7). At the east of the surface front, associated with the intense southeasterly winds, the evaporation is strongly decreased in COA (Figure 8b). On the contrary, the latent heat flux values in COA experiment are larger at the west of the surface front, where low-level wind is weak. As for the Aude case, small local differences in sensible and latent heat fluxes are visible within the convective region (Figure 8).

[31] In every case studied, using the COARE 3.0 algorithm decreases the simulated momentum flux. For example, Figure 9 plots for the Hérault case the values of latent heat, sensible heat and momentum fluxes at each sea grid points of the 2.4 km domain for both ORI and COA simulations. Figure 9a shows that differences in momentum flux over the sea surface can be very important between the two parameterizations in high-wind regime: up to -5.6 N m^{-2} simulated by ORI for $u = 32 \text{ m s}^{-1}$ against only -1.6 N m^{-2} simulated by COA. Values of stress simulated by the original MESO-NH parameterization, of more than $3\text{--}4 \text{ N m}^{-2}$ in absolute value, seems to be overestimated [Eymard *et al.*, 1999; Caniaux *et al.*, 2005] and could have a strong impact from an oceanic point of view. The differences in term of sensible heat flux between the ORI and COA simulations (Figure 9b) show that the COARE 3.0 algorithm decreases H in absolute value but the averaged values over the domain are nearly the same. Figure 9c shows clearly the two areas with different conditions in low-level winds on both sides of the surface front (regions labeled R and L in Figure 8b and in Figure 9c). It is interesting to note that large differences can be encountered in LE between the two parameterizations not only in strong wind regimes ($> 20 \text{ m s}^{-1}$), but also in moderate wind regimes ($< 12 \text{ m s}^{-1}$) when is present a large vertical gradient in moisture between sea and the lowest model level.

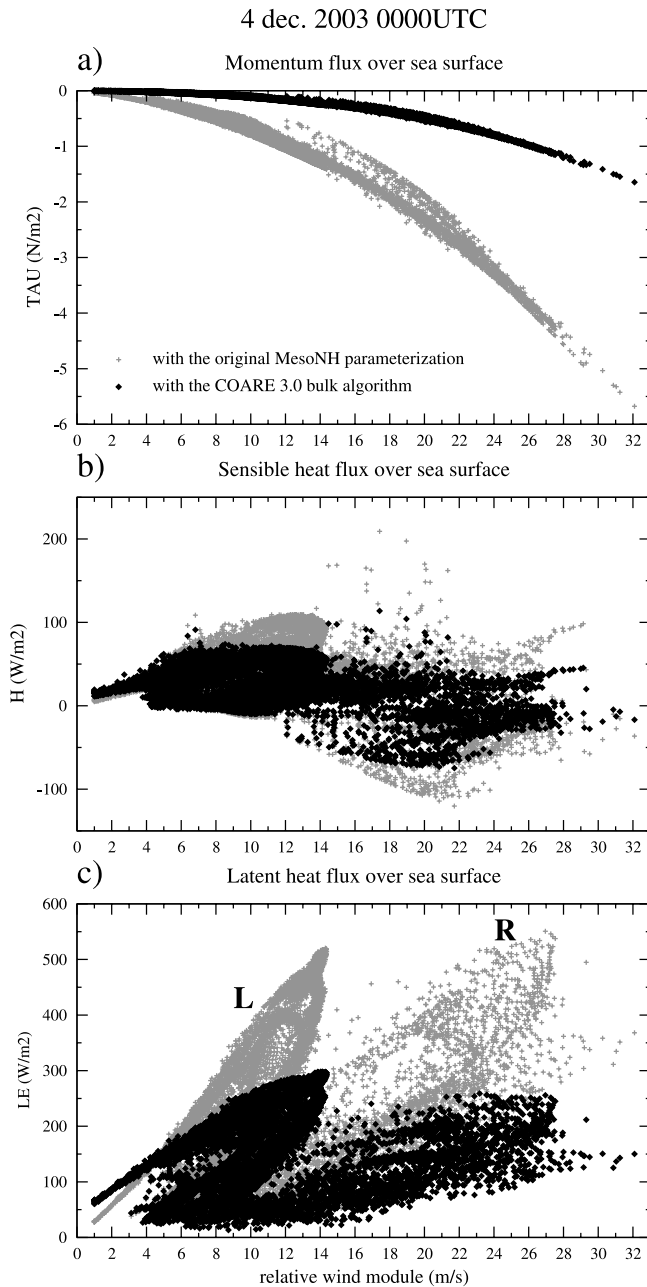


Figure 9. HERAULT CASE, 0000 UT, 4 December 2003: (a) momentum flux (τ in N m^{-2}), (b) sensible heat flux (H in W m^{-2}), and (c) latent heat flux (LE in W m^{-2}) for all the 2.4-km domain sea grid points from ORI (in grey) and COA (in black), in function of the relative wind speed.

4.2. Boundary Layer

[32] Figure 10 shows the 30-m AGL vapor mixing ratio and temperature averaged over the sea grid points of the 2.4 km MESO-NH domain for the Aude case. As a result of the strong decrease in average of the latent heat flux over the sea, the atmospheric low levels contain less vapor in

COA experiment (about 0.2 g kg^{-1} in average). The 30-m AGL mean temperature is also colder for COA, the difference reaching about 0.1°C at the end of the simulation. This results from a reduction in average of the sum of the two turbulent heat fluxes ($H + LE$). Figure 11 shows the equivalent potential temperature average over the sea domain after 15 hours of simulation for the three cases and the two experiments. As a result of less moistened and colder low levels for the Aude case, the mean vertical profile is less unstable in COA, which is less favorable therefore to deep convection. This decrease of equivalent potential temperature up to 2000 m in COA compared to ORI experiment is of the same order than the one obtained by a mean SST decrease of 1.5°C (see LE06), leading to a significant reduction of the convective activity. For the Gard case, no difference is found for the mean equivalent potential temperature profile (Figure 11), and we can therefore expect almost no difference in terms of simulation of the precipitating system (see section 4.3). For the Hérault case, as during the morning and up to 1500 UT, both latent and sensible heat fluxes are more important in COA, the COA mean profile at 1500 UT is slightly more unstable.

[33] Whereas significant differences in wind stress have been shown for high winds, the impact on the average values of low-level winds is weak (Figure 7). The COA experiment tends to produce weaker low-level winds, except during the afternoon of 3 December 2003 for the Hérault case. The differences are mainly concentrated within the precipitating region. As instance, for the Aude case, except underneath the precipitating system where differences can reach 5 m s^{-1} (Figure 12), the low-level flow is not affected elsewhere by the change of parameterization, even in the low-level jet area. Wind differences within the precipitating areas are again induced by slight differences in convective cells location, resulting in differences in the location of the gusty winds underneath the convective cells.

4.3. Convective Systems and Associated Surface Rainfall

[34] The simulations both succeeded in simulating well-developed and quasi-stationary MCSs for the Aude and Gard cases and a quasi-stationary frontal system for the Hérault case. Objective scores computed on the whole simulation period against rain gauge observations show that MESO-NH performs better for the Hérault and Aude cases than for the Gard case (Table 2). The weak Equitable Threat Score and correlation coefficient for the Gard case are explained by an error in location of about 80 km of the heaviest precipitation area associated with the MCS. Using ARPEGE analysis at different times (0000 or 0600 UT) leads to the same drawback. A better localization of the precipitation maximum can be obtained by applying a mesoscale data analysis to produce the initial conditions [Chancibault *et al.*, 2006; Nuissier *et al.*, 2008]. However, in order to have the same experimental framework for the three cases allowing intercomparison, we have chosen here to start all the simulations from an ARPEGE analysis. Note, however, that the simulation of the Gard case places the precipitation maximum over a region that is typically affected by these types of events, i.e., the Cévennes-Vivarais region (Figure 13). Therefore, the simulated rainfall

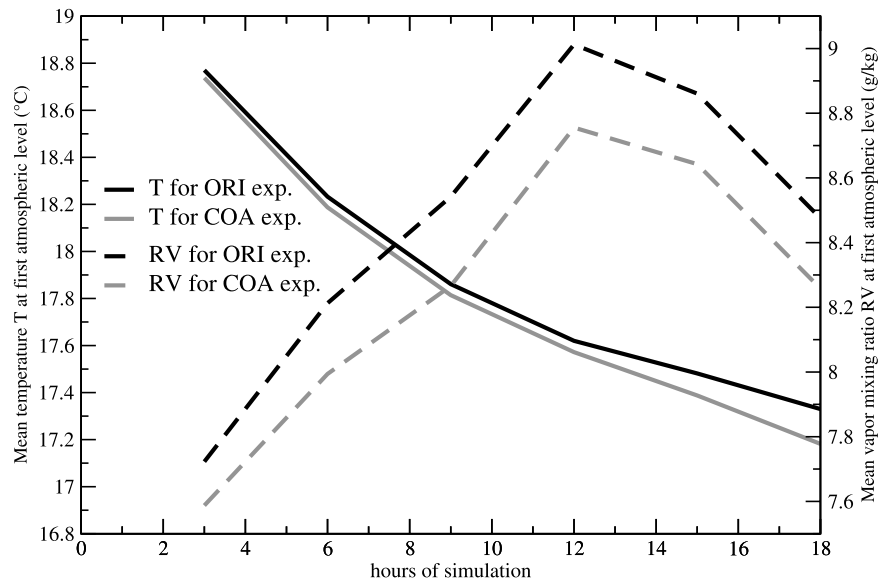


Figure 10. AUDE CASE: Temporal evolution of the 30-m AGL mean temperature and mean vapor mixing ratio over the 2.4-km sea domain.

episode can be nonetheless considered as representative of torrential events occurring in this area. For the two other cases, the objective scores show quite good ETS for significant precipitation (Table 2). For the Hérault flooding case, the simulations reproduce almost perfectly the frontal system with embedded convection extended over the Gulf of Lions and the associated strong low-level wind convergence. Moderate to intense southeasterly low-level winds are simulated on the eastern side of the front that progressed

westward. They reach locally 20 m s^{-1} in the first part of the day, before increasing to about 30 m s^{-1} after 1400 UT. Comparison to the observed 24-h accumulated precipitation shows that the simulations perform well with a high coefficient correlation and a bias of only 1.8 mm (Table 2). This weak overestimation is due to a slightly slower westward progress of the frontal system compared to the observed system. A detailed description of the results of these simulations is given by LE06.

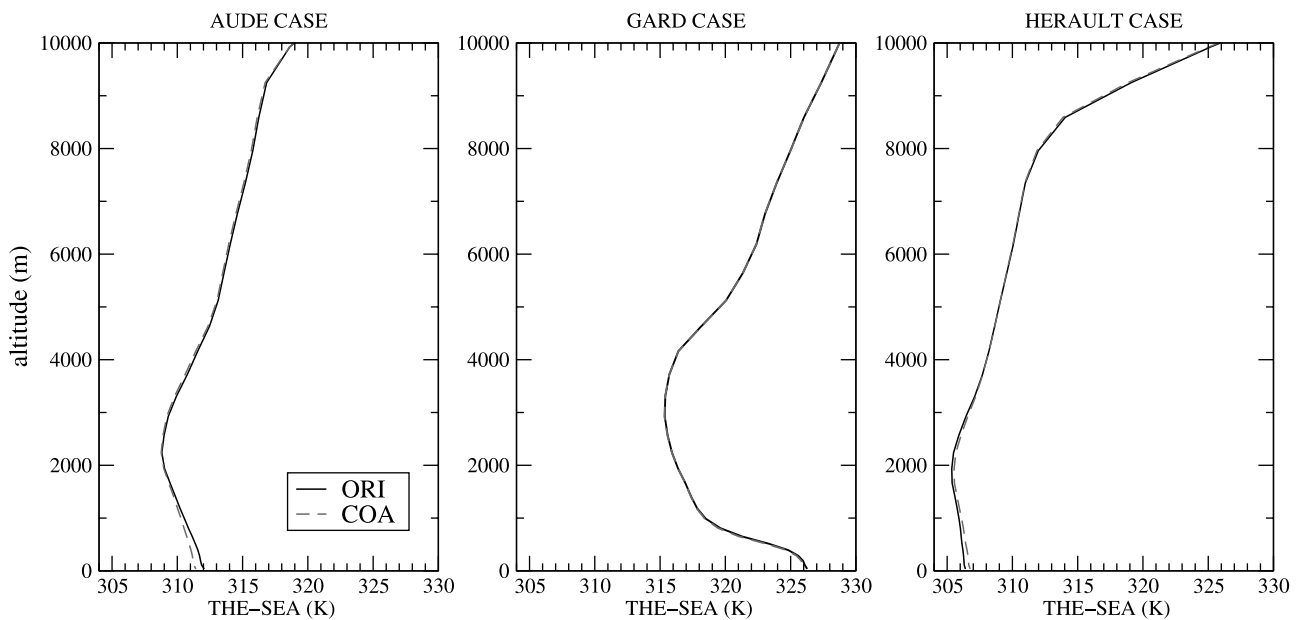


Figure 11. Vertical profiles of equivalent potential temperature (K) averaged over sea surface of the 2.4-km grid for ORI and COA experiments: for (left) the Aude case at 0300 UT, 13 November 1999, (middle) the Gard case at 0300 UT, 9 September 2002, and (right) the Hérault case at 1500 UT, 3 December 2003.

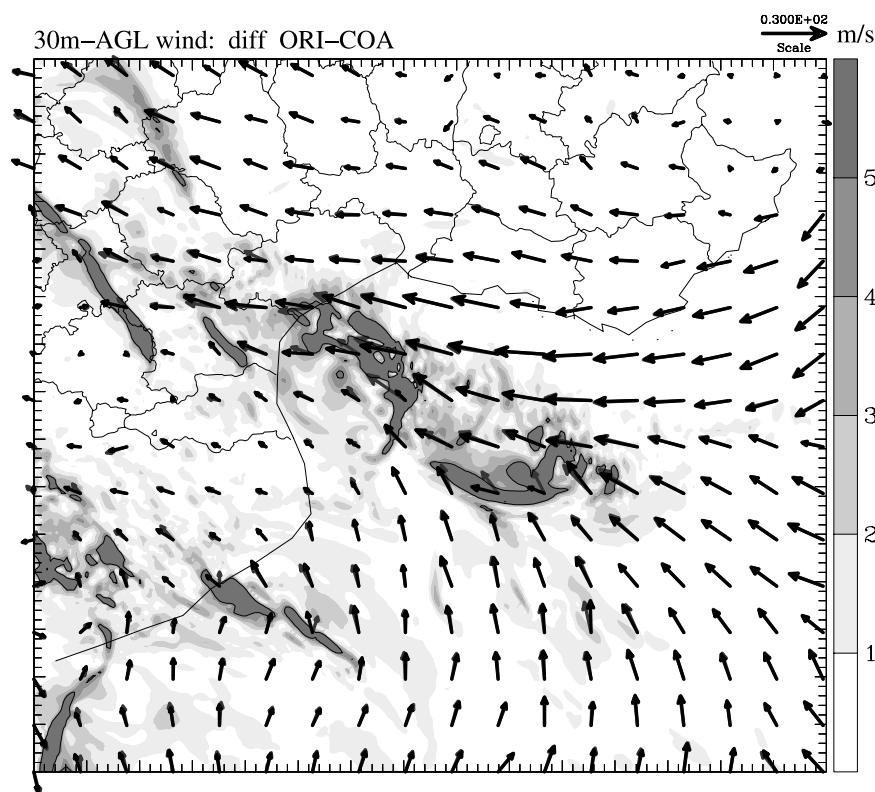


Figure 12. AUDE CASE, 0600 UT, 13 November 1999: 30-m AGL wind differences (m s^{-1}) between ORI and COA experiments superimposed to 30-m AGL wind vectors simulated by ORI (black arrows) and COA (grey arrows). Differences larger than 5 m s^{-1} are delineated by solid lines.

[35] For the three cases, using the COARE 3.0 parameterization results in a reduction of the maximum of precipitation by 5 to 10% (Table 2). For the Gard case, ORI and COA are very close in term of location of the convective system (Figure 13) and accumulated precipitation (Figure 14) as expected by the small differences in term of low-level atmospheric conditions. For the Aude case, weaker latent heat fluxes and less unstable low levels result in a decrease by about 10% of the precipitation amounts (Figure 14) and of its maximum (Table 2), without having a significant impact on the location of the convective system (Figure 6). For the Hérault case, even though the western side of the surface front is more unstable up to 1500 UT in COA, the strong decrease of the evaporation for the eastern side of the surface front where occurred the intense southeasterly

winds (Figure 8b) results in weaker moisture and convective energy available for the deep convection in the last part of the day. For that case, the motion speed of the frontal system is also slightly modified, with a faster eastward progress of the frontal system in COA (Figure 15). This faster progress caused by a less intense embedded convection within the front was already found in an experiment with a colder SST, which acts in decreasing the evaporation during the simulation (see LE06 study for more details). Consequently, although the mean precipitation surface totals on the domain are very close between the two experiments (Figure 14), the maximum value of 24-h precipitation totals is lower by 18 mm in COA compared to ORI (Table 2). Scores against the observations show that for that case the 24-h precipitation totals simulated by COA are slightly improved, with

Table 2. Maximum Accumulated Surface Rainfall Simulated for the Total Simulation Duration and Scores Against Rain Gauges Rainfall Accumulated Over the Whole Duration of the Simulation^a

Parameterization	Maximum Accumulated Rainfall (mm)	Scores				
		ETS	Correlation	Bias	RMS	
Aude case	ORI	296	0.65	0.55	-3.5	33.8
	COA	265	0.63	0.57	-5.2	32.5
Gard case	ORI	396	0.22	0.25	-7.1	53.3
	COA	368	0.22	0.23	-6.8	55.3
Hérault case	ORI	306	0.61	0.81	1.8	22.9
	COA	288	0.64	0.82	1.6	21.2

^aUnit is millimeters. Duration of simulation: 18 h for the Aude case and 24 h for the Gard and the Hérault cases. Equitable Threat Score (ETS) [Gandin and Murphy, 1992] is presented for the 20-mm threshold.

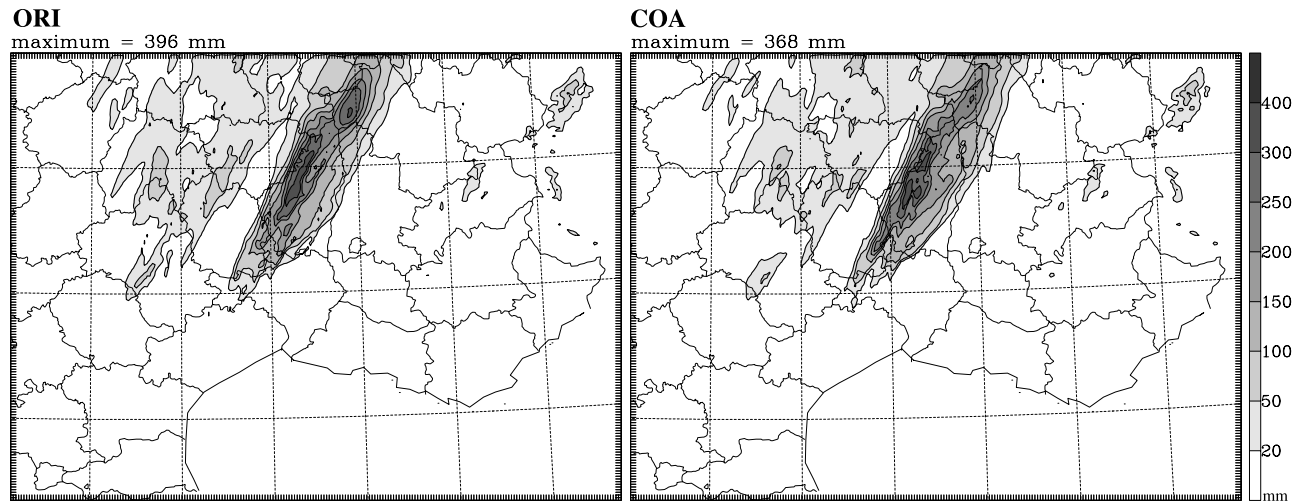


Figure 13. GARD CASE: 24-h accumulated precipitation (millimeters) simulated by (left) ORI and (right) COA from 1200 UT, 8 September 2002 to 1200 UT, 9 September 2002.

reduced bias and root mean square and higher correlation and ETS.

5. Impact on the Ocean Mixed Boundary Layer

[36] The impact of the surface fluxes parameterization on the ocean mixed boundary layer is now examined. The 1-D oceanic model has been driven by the surface fluxes computing from the atmospheric parameters simulated by the reference MESO-NH simulation (ORI) at 1200 UT, 3 December 2003 for each grid points of the area delineated in Figure 16. The turbulent fluxes computing either by the COARE3.0 or original MESO-NH parameterizations according to these atmospheric data (low-level temperature, humidity and wind), the infrared radiation and the precipitation rate are kept constant and imposed all along the 24 hours run to the oceanic model. Only a diurnal variation of the solar radiation is imposed.

[37] The oceanic model is initialized with the MERCATOR analysis at 0000 UT, 3 December 2003. Results are compared to the MERCATOR analysis at 0000 UT, 4 December 2003. Within the domain on which the ocean model is run, the low-level winds exhibit a strong gradient and SST is rather cold.

[38] Figure 17a shows the salinity and temperature oceanic profiles after 24 hours of simulation averaged over the simulation domain (272 grid points, black box drawn in Figure 16), whereas Figure 17b displays the same parameters for a specific ocean column (white bullet in Figure 16) which is located under the low-level jet and characterized by a relative cold SST and a large vertical temperature gradient between the surface and the atmospheric low levels. The comparison to the initial and final MERCATOR profiles clearly shows that the temperature and the salinity profiles better fit the final MERCATOR profiles when the 1-D oceanic model is driven by the COARE 3.0 surface fluxes. The original MESO-NH parameterization producing larger latent heat and momentum surface fluxes in high-wind regime significantly overestimates the vertical turbulent mixing in the OML with an oceanic mixed layer deepening by about 50 m and a temperature decrease by

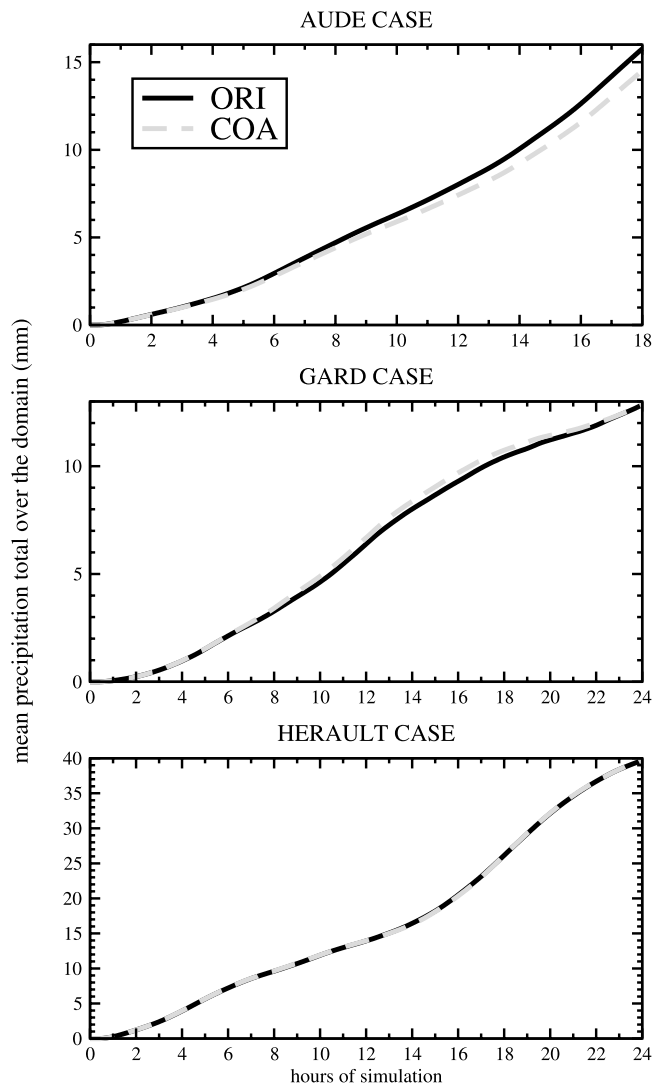


Figure 14. Temporal evolution of the surface precipitation totals accumulated since the beginning of the simulation and averaged over the 2.4-km domain sea grid points for the (top) Aude, (middle) Gard, and (bottom) Hérault cases.

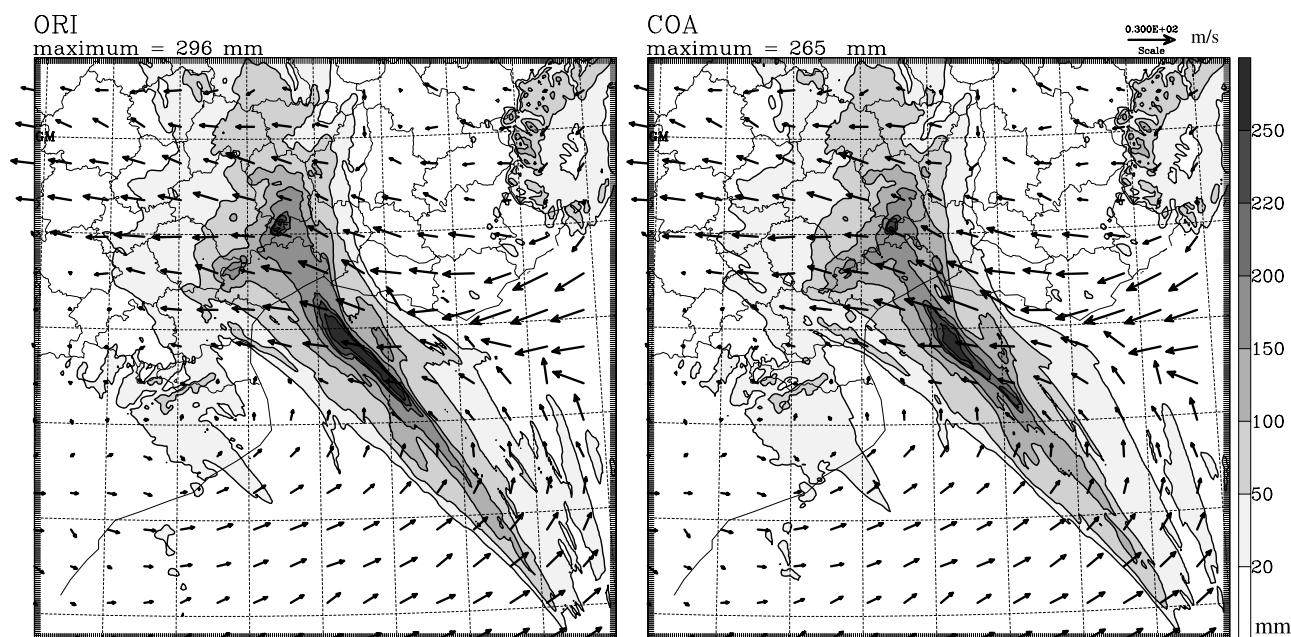


Figure 15. HERAULT CASE: 24-h accumulated precipitation (millimeters) simulated by (left) ORI and (right) COA from 0000 UT, 3 December 2003 to 0000 UT, 4 December 2003, superimposed to the 30-m AGL winds at 0000 UT, 4 December 2003.

0.3°C in 24 hours under the low-level jet (Figure 17b). Using the original MESO-NH parameterization significantly alters the salinity profiles, with large differences from both the initial and final MERCATOR profiles (Figure 17). Table 3 presents the bias and root mean square scores for the ocean mixed layer depth computed against the MERCATOR profiles at 0000 UT, 4 December over the whole domain on which the 1-D ocean model has been run. Clearly, these scores confirm that COARE3.0 provides a better fit to the MERCATOR profiles.

[39] The above described experiment used a single diurnal atmospheric data set as often done to drive regional high-resolution oceanic models. Additional oceanic simulations using higher temporal resolution of atmospheric forcing issued from the MESO-NH simulations (in particular with a three hourly forcing time evolution; not shown) lead to the same conclusions, i.e., a stronger cooling and deepening under the low-level jet when the *Louis* [1979] parameterization is used. Conclusions of these oceanic simulations are therefore that large differences in the ocean mixed layer simulation can be obtained locally when using different sea fluxes parameterizations.

6. Conclusion

[40] The sensitivity of high-resolution atmospheric forecast of Mediterranean torrential rain events to the sea surface fluxes parameterization has been evaluated. Two different sea surface fluxes parameterizations have been used for three torrential rain events over southeastern France: the original sea surface fluxes parameterization of the MESO-NH model [*Louis*, 1979] and a slightly simplified version the COARE 3.0 bulk parameterization [*Fairall et al.*, 2003]. The iterative COARE bulk algorithm and the

original MESO-NH parameterization produce very different sea surface turbulent fluxes values especially for latent heat flux and momentum flux in intense to severe wind regimes.

[41] As the latent heat fluxes is strongly decreased specially under the strong low-level winds when the COARE algorithm is used, it results in average in dryer and less unstable atmospheric boundary layers over the Mediterranean Sea. The deep convection is therefore a little less intense and surface rainfall totals weaker. The largest differences are found for the torrential rain event with the strongest low-level jet, i.e., the Aude case. Even if the maximum accumulated rainfall is decreased in COA experiments for every case studied, the convective activity simulated is still intense and representative of Mediterranean heavy rain events. Scores against observed rainfall totals show an improvement for the Hérault cases when using the COARE algorithm, whereas the impact is almost neutral for the two other cases. Generally, the loss of energy induced by the change of parameterization from ORI to the COARE algorithm, has the same effects on the atmospheric convection than experiences where the SST is decreased by 1.5°C by LE06.

[42] Even though using the COARE algorithm does not improved systematically the short-range high-resolution atmospheric convection forecast, the strong differences of momentum fluxes over sea surface between the two parameterizations could be very important for the oceanic dynamics. Indeed, values of stress simulated by the original MESO-NH parameterization in high-wind regime (nearly -6 N m^{-2} for $u_{10m} > 30 \text{ m s}^{-1}$) are probably overestimated and could produce an exaggerated mixing of the ocean upper layers. The COARE parameterization produces significantly weaker values in high-wind regime, so the mixing and the cooling of the upper ocean are expected to be more realistic. This has been checked by driving a 1-D oceanic model with

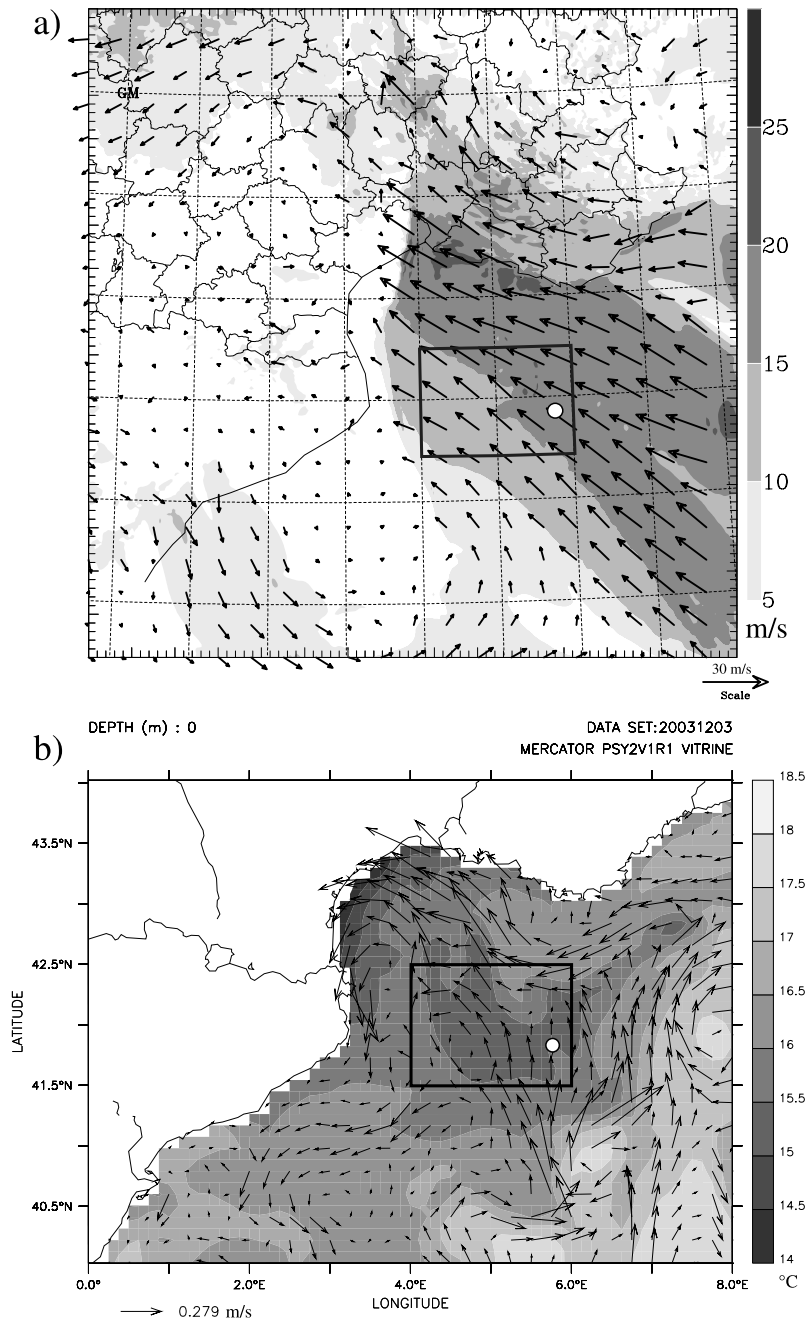


Figure 16. HERAULT CASE: oceanic conditions and atmospheric forcing imposed on the 1-D oceanic model: (a) 30-m AGL winds (m s^{-1}) at 1200 UT, 3 December 2003 and (b) analyzed MERCATOR SST ($^{\circ}\text{C}$) and surface current (m s^{-1}) for 3 December 2003. The 1-D oceanic model is run for grid points in the area delineated by the black box.

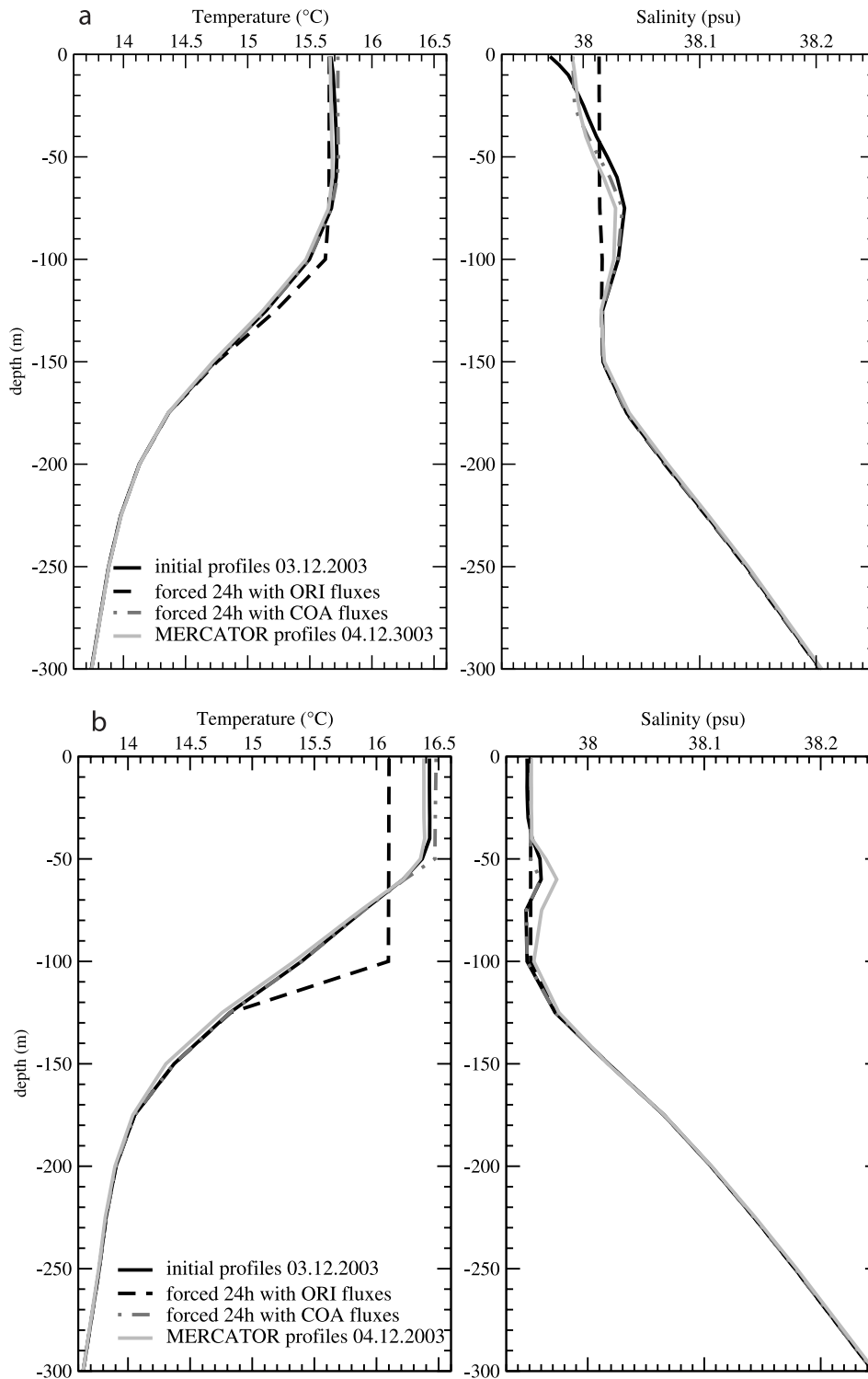


Figure 17. Temperature and salinity profiles (a) averaged over all grid points contained within the box displayed in Figure 16 and (b) at the grid point indicated by a white bullet in Figure 16.

fluxes simulated by the two parameterizations for the Hérault case. The next step of this study is to develop a full two-way coupling between the MESO-NH model and this one-dimensional oceanic model to evaluate the interaction and feedbacks occurring during the Mediterranean

Table 3. Bias and RMS for the Ocean Mixed Layer Depth Against the MERCATOR Profiles at 0000 UT, 4 December 2003 Over the Domain Shown in Figure 16

		ORI	COA
Mixed layer	BIAS	10.7	-4.8
Depth (m)	RMS	17.9	14.6

heavy precipitating events and also during the preconditioning of their mesoscale low-level environment.

Appendix A

A1. Insights of the COARE 3.0 Bulk Algorithm

[43] In the COARE3.0 bulk algorithm, the transfer coefficients C_x are expressed as

$$C_X = \frac{u_* X_*}{S \Delta X} = c_x^{1/2} c_d^{1/2} \quad (\text{A1})$$

$$c_x^{1/2} c_d^{1/2} = c_{xn}^{1/2} F_x(\zeta) c_{dn}^{1/2} F_d(\zeta), \quad (\text{A2})$$

where

$$F_x(\zeta) = \frac{\ln\left(\frac{z}{z_{0x}}\right)}{\ln\left(\frac{z}{z_{0x}}\right) - \psi_x(\zeta)}. \quad (\text{A3})$$

[44] The iterative method in the COARE 3.0 algorithm determines the scaling parameters u_* , θ_* and q_* from the MOST stability parameter $\zeta = z/L$ with L the Monin-Obukhov scale height given by

$$(z/L)^{n+1} = \zeta^{n+1} = g(u_*^n, \theta_*^n, q_*^n)$$

$$L^{n+1} = \frac{T}{\kappa g} \frac{u_*^{n2}}{\theta_*^n + 0.61 T q_*^n}.$$

The new scaling parameters are then expressed from the flux-profile relationships between the roughness length z_0 and the height z of the lowest model level according to equation (A2),

$$u_*^{n+1} = \frac{\kappa S}{\ln\left(\frac{z}{z_0}\right) - \psi_m(\zeta^{n+1})} \quad (\text{A4})$$

$$\theta_*^{n+1} = \frac{\kappa(\theta_a - \theta_s)}{\ln\left(\frac{z}{z_0}\right) - \psi_h(\zeta^{n+1})} \quad (\text{A5})$$

$$q_*^{n+1} = \frac{\kappa(q_a - q_s)}{\ln\left(\frac{z}{z_0}\right) - \psi_h(\zeta^{n+1})} \quad (\text{A6})$$

ψ_m and ψ_h are modified *Businger et al.*'s [1971] functions given by the following:

$$\psi_m(\zeta) = \begin{cases} -(1 + \zeta)^1 - 0.6667 \frac{(\zeta - 14.28)}{\exp(\Gamma)} - 8.525 & \text{stable}(\zeta \geq 0) \\ (1 - f)\psi_{mK} + f\psi_{mC} & \text{unstable}(\zeta < 0) \end{cases} \quad (\text{A7})$$

$$\Gamma = \min(50, 0.35\zeta)$$

$$\begin{cases} c_d = c_{dn} \times \mathcal{F}_d^2(Ri, z, z_0, z_{0h}) \\ c_h = c_{dn}^{\frac{1}{2}} c_{hn}^{\frac{1}{2}} \times \mathcal{F}_d(Ri, z, z_0, z_{0h}) \mathcal{F}_h(Ri, z, z_0, z_{0h}) = c_{dn}^{\frac{1}{2}} c_{hn}^{\frac{1}{2}} \times (\mathcal{F}_h'(Ri, z, z_0, z_{0h}))^2 \end{cases} \quad (\text{A10})$$

$$f = \frac{\zeta^2}{(1 + \zeta^2)}$$

$$\psi_{mK} = 2\ln\left(\frac{1+x}{2}\right) + \ln\left(\frac{1+x^2}{2}\right) - 2\arctan(x) + \frac{\pi}{2}$$

$$x = (1 - 15\zeta)^{\frac{1}{2}}$$

$$\psi_{mC} = \frac{3}{2}\ln\left(\frac{y^2 + y + 1}{3}\right) - \sqrt{3}\arctan\left(\frac{2y + 1}{\sqrt{3}}\right) + \frac{\pi}{\sqrt{3}}$$

$$y = (1 - 10.15\zeta)^{\frac{1}{3}}$$

$$\psi_h(\zeta) = \begin{cases} -(1 + \frac{2}{3}\zeta)^{1.5} - 0.6667 \frac{(\zeta - 14.28)}{\exp(\Gamma)} - 8.525 & \text{stable}(\zeta \geq 0) \\ (1 - f)\psi_{hK} + f\psi_{hC} & \text{unstable}(\zeta < 0) \end{cases} \quad (\text{A8})$$

$$\Gamma = \min(50, 0.35\zeta)$$

$$f = \frac{\zeta^2}{(1 + \zeta^2)}$$

$$\psi_{hK} = 2\ln\left(\frac{1+x}{2}\right)$$

$$x = (1 - 15\zeta)^{\frac{1}{2}}$$

$$\psi_{hC} = \frac{3}{2}\ln\left(\frac{y^2 + y + 1}{3}\right) - \sqrt{3}\arctan\left(\frac{2y + 1}{\sqrt{3}}\right) + \frac{\pi}{\sqrt{3}}$$

$$y = (1 - 34.15\zeta)^{\frac{1}{3}}$$

A2. Insights of the Original MESO-NH Air-Sea Fluxes Parameterization

[45] In the original MESO-NH parameterization, the exchange coefficients (equation (5)) are directly determined from *Louis's* [1979] functions \mathcal{F}_x according to the Richardson number R_i that replaces here the MOST stability parameter, the level height and the roughness lengths,

$$c_x^{1/2}(\zeta) = c_{xn}^{1/2} \mathcal{F}_x(Ri, z, z_0, z_{0h}) \quad (\text{A9})$$

The stability parameter (z_0) and function \mathcal{F}'_e for evaporation are imposed to be identical to heat stability parameter and function so that the exchange coefficient for the latent heat flux c_e is equal to c_h .

[46] The Louis's [1979] functions \mathcal{F}_d and \mathcal{F}'_h are given by

$$\mathcal{F}_d(Ri, z, z_0, z_{0h}) = \begin{cases} \left(\frac{1}{1 + \frac{10Ri}{\sqrt{1+5Ri}}} \right)^{\frac{1}{2}} & \text{stable } (Ri > 0) \\ \left(1 - \frac{10Ri}{1 + C_m \sqrt{-Ri}} \right)^{\frac{1}{2}} & \text{unstable } (Ri \leq 0) \end{cases} \quad (A11)$$

$$C_m = 10c_m^* c_{dn} \left(\frac{z}{z_0} \right)^{p_m}$$

$$c_m^* = 6.8741 + 2.6933\mu - 0.3601\mu^2 + 0.0154\mu^3$$

$$p_m = 0.5233 - 0.0815\mu + 0.0135\mu^2 - 0.0010\mu^3$$

$$\mathcal{F}'_h(Ri, z, z_0, z_{0h}) = \begin{cases} \left(\frac{1}{1 + 15Ri\sqrt{1+5Ri}} \right)^{\frac{1}{2}} & \text{stable } (Ri > 0) \\ \left(1 - \frac{15Ri}{1 + C_h \sqrt{-Ri}} \right)^{\frac{1}{2}} & \text{unstable } (Ri \leq 0) \end{cases} \quad (A12)$$

$$C_h = 15c_h^* c_{dn}^{\frac{1}{2}} c_{hn}^{\frac{1}{2}} \left(\frac{z}{z_0} \right)^{p_h}$$

$$c_h^* = 3.2165 + 4.3431\mu + 0.5360\mu^2 - 0.0781\mu^3$$

$$p_h = 0.5802 - 0.1571\mu + 0.0327\mu^2 - 0.0026\mu^3$$

with $\mu = \ln \left(\frac{z_0}{z_{0h}} \right)$.

[47] **Acknowledgments.** This work is a contribution to the French project "CYclogénèse et PRécipitations Intenses en Méditerranée" (CYP-RIM) sponsored by the ACI-FNS "Aléas et Changements Globaux." We gratefully acknowledge Chris Fairall, who gave us the online access to the COARE algorithm. We also thank Sophie Belamari and Guy Caniaux for their help in bulk algorithms understanding and Patrick Lemoigne for his help in the software implementation. The authors are grateful to the three anonymous reviewers, who provided us useful recommendations.

References

Bahurel, P., E. Dombrowsky, and J.-M. Lellouche (2004), Mercator ocean monitoring and forecasting system, near-realtime assimilation of satellite and in-situ data in different operational ocean models, paper presented at 36th International Liège Colloquium on Ocean Dynamics, Liège, Belgium.

Bechtold, P., E. Bazile, F. Guichard, P. Mascart, and E. Richard (2001), A mass-flux convection scheme for regional and global models, *Q. J. R. Meteorol. Soc.*, *127*, 869–886.

Brunke, M. A., X. Zeng, and S. Anderson (2002), Uncertainties in sea surface turbulent flux algorithms and data sets, *J. Geophys. Res.*, *107*(C10), 3141, doi:10.1029/2001JC000992.

Brunke, M. A., C. W. Fairall, X. Zeng, L. Eymard, and J. A. Curry (2003), Which bulk aerodynamic algorithms are least problematic in computing ocean surface turbulent fluxes?, *J. Clim.*, *16*, 619–635.

Businger, J. A., J. C. Wyngaard, Y. Izumi, and E. Bradley (1971), Flux profile relationship in the atmospheric surface layer, *J. Atmos. Sci.*, *28*, 181–189.

Caniaux, G., A. Brut, D. Bourras, H. Giordani, A. Paci, L. Prieur, and G. Reverdin (2005), A 1-year sea surface heat budget in the northeastern Atlantic basin during the POMME experiment: 1. Flux estimates, *J. Geophys. Res.*, *111*, C07S02, doi:10.1029/2004JC002596.

Chancibault, K., S. Anquetin, V. Ducrocq, and G.-M. Saulnier (2006), Hydrological evaluation of high-resolution precipitation forecast of the Gard flash-flood event (8–9 September 2002), *Q. J. R. Meteorol. Soc.*, *132*, 1091–1118.

Charnock, H. (1955), Wind stress on a water surface, *Q. J. R. Meteorol. Soc.*, *81*, 639–640.

Delrieu, G., et al. (2005), The catastrophic flash-flood event of 8–9 September 2002 in the Gard region, France: A first case study for the Cévennes-Vivarais Mediterranean Hydrometeorological Observatory, *J. Hydrometeorol.*, *6*, 34–52.

Ducrocq, V., D. Ricard, J.-P. Lafore, and F. Orain (2002), Storm-scale numerical rainfall prediction for five precipitating events over France: On the importance of the initial humidity field, *Weather Forecasting*, *17*(6), 1236–1256.

Ducrocq, V., K. Chancibault, F. Habets, and S. Anquetin (2003), Meso-scale modelling of a flooding storm: Application to the extreme flood of Gard, paper presented at 5th Plinius Conference on Mediterranean Storms, Eur. Geophys. Soc., Ajaccio, France.

Ekman, V. W. (1905), On the influence of the Earth's rotation on ocean currents, *Ark. Mat. Astron. Fys.*, *2*, 1–53.

Eymard, L., et al. (1999), Surface fluxes in the North Atlantic current during CATCH/FASTEX, *Q. J. R. Meteorol. Soc.*, *125*, 3563–3599.

Fairall, C. W., E. F. Bradley, D. P. Rogers, J. B. Edson, and G. S. Young (1996), Bulk parameterization of air-sea fluxes for Tropical Ocean-Global Atmosphere Coupled-Ocean Atmosphere Response Experiment, *J. Geophys. Res.*, *101*(C2), 3747–3764.

Fairall, C. W., A. B. White, J. B. Edson, and J. E. Hare (1997), Integrated shipboard measurements of the marine boundary layer, *J. Atmos. Oceanic Technol.*, *14*(3), 338–359.

Fairall, C. W., E. F. Bradley, J. E. Hare, A. A. Grachev, and J. B. Edson (2003), Bulk parameterization of air-sea fluxes: Updates and verification for the COARE algorithm, *J. Clim.*, *16*, 571–591.

Gandin, L. S., and A. H. Murphy (1992), Equitable skill scores for categorical forecasts, *Mon. Weather Rev.*, *120*, 361–370.

Gaspar, P., Y. Grgoris, and J.-M. Lefevre (1990), A simple Eddy Kinetic Energy model for simulations of the oceanic vertical mixing: Tests at station Papa and Long-Term Upper Ocean Study site, *J. Geophys. Res.*, *95*(C9), 16,179–16,193.

Giordani, H., and G. Caniaux (2001), Sensivity of cyclogenesis to sea surface temperature in the Northwestern Atlantic, *Mon. Weather Rev.*, *129*, 1273–1295.

Giordani, H., L. Prieur, and G. Caniaux (2006), Advanced insights into sources of vertical velocity in the ocean, *Ocean Dyn.*, *56*(5-6), 513–524, doi:10.1007/s10236-005-0050-1.

Gosnell, R., C. Fairall, and P. J. Webster (1995), The sensible heat of rainfall in the tropical ocean, *J. Geophys. Res.*, *100*(C9), 18,437–18,442.

Kraus, E. B. (1972), *Atmosphere-Ocean Interactions*, 352 pp. Oxford Univ. Press, London.

Lafore, J.-P., et al. (1998), The Meso-NH Atmospheric Simulation System. Part I: Adiabatic formulation and control simulations. Scientific objectives and experimental design, *Ann. Geophys.*, *16*(1), 90–109.

Lebeaupin, C., V. Ducrocq, and H. Giordani (2006), Sensitivity of torrential rain events to the sea surface temperature based on high-resolution numerical forecasts, *J. Geophys. Res.*, *111*, D12110, doi:10.1029/2005JD006541.

Louis, J.-F. (1979), A parametric model of vertical eddy fluxes in the atmosphere, *Boundary Layer Meteorol.*, *17*, 187–202.

Masson, V. (2000), A physically-based scheme for urban energy balance in atmospheric models, *Boundary Layer Meteorol.*, *94*, 357–397.

Monin, A. S., and A. M. Obukhov (1954), Basic regularity in turbulent mixing in the surface layer of the atmosphere, *Dokl. Akad. Nauk. SSSR*, *24*, 163–187.

Noilhan, J., and J. F. Mahfouf (1996), The ISBA land surface parameterization scheme, *Global Planet. Change*, *13*, 145–159.

Nuissier, O., V. Ducrocq, D. Ricard, C. Lebeaupin, and S. Anquetin (2008), A numerical study of three catastrophic precipitating events over western Mediterranean region (southern France). part I: Numerical framework and synoptic ingredients, *Q. J. R. Meteorol. Soc.*, *134*, 111–130.

Pinty, J.-P., and P. Jabouille (1998), A mixed-phase cloud parameterization for use in a mesoscale non-hydrostatic model: Simulations of a squall line of orographic precipitation, paper presented at Conference on Cloud Physics, Am. Meteorol. Soc., Everett, Wash.

- Smith, S. (1988), Coefficients for sea surface wind stress, heat fluxes and wind profiles as a function of wind speed and temperature, *J. Geophys. Res.*, *93*(C12), 15,467–15,472.
- Webb, E. K., G. I. Pearman, and R. Leuning (1980), Correction of flux measurements for density effects due to heat and water vapour transfer, *Q. J. R. Meteorol. Soc.*, *106*, 85–100.
- Webster, P. J., and R. Lukas (1992), TOGA COARE: The coupled ocean-atmosphere response experiment, *Bull. Am. Meteorol. Soc.*, *73*(9), 1377–1416.
- Weill, A., et al. (2003), Toward better determination of turbulent air-sea fluxes from several experiments, *J. Clim.*, *16*, 600–618.
- Weller, R. A., F. Bradley, and R. Lukas (2004), The interface or air-sea fluxes component of the TOGA Coupled Ocean-Atmosphere Response Experiment and its impact on subsequent air-sea interactions studies, *J. Atmos. Oceanic Technol.*, *21*, 223–257.
-
- V. Ducrocq, H. Giordani, and C. Lebeau-pin Brossier, CNRM/GAME, 42 avenue G. Coriolis, F-31057 Toulouse CEDEX, France. (cindy.lebeau-pin@lmd.polytechnique.fr)